GMR
The Original

GREEN SYNTHESIS OF CUO NANOPARTICLES LOADED WITH POLYMERIC NANOSCAFFOLDS FROM *SARGASSUM WIGHTII* EXTRACT FOR ENHANCED ANTICANCER ACTIVITY ON HT-29 AND MCF-7 CELLS

Karneesh Kumar[1], Sanjay Surya R[2], Alagendran Subbarayalu[3]*, Chella Perumal Palanisamy[4]*

[1]Saveetha Medical College & Hospital (SMCH), Saveetha Institute of Medical and Technical Sciences (SIMATS), Thandalam, Chennai, Tamil Nadu 602105, India. kkarneesh8@gmail.com
[2]Department of Anaesthesiology, Saveetha Medical College and Hospital, Saveetha Institute of Medical And Technical Sciences (SIMATS), Thandalam, Chennai-602105, Tamil Nadu, India. Email: sanjaysurya1997@gmail.com; ORCID: https://orcid.org/0009-0005-9187-8496.
[3]Clinical Neuroscience and Phytomedicine Laboratory, Department of Research, Saveetha College of Nursing (SCON), Saveetha Institute of Medical and Technical Sciences (SIMATS), Chennai 602105, Tamil Nadu, India. Email: proteinblg@gmail.com; alagendrans.scon@saveetha.com. ORCID: https://orcid.org/0009-0009-0749-7180.
[4]Phytochemistry and Pharmacotherapy Laboratory, Department of Dermatology, Saveetha Medical College & Hospital (SMCH), Saveetha Institute of Medical and Technical Sciences (SIMATS), Thandalam, Chennai, Tamil Nadu 602105, India. chellaperumalp.smc@saveetha.com
*Correspondence: chellaperumalp.smc@saveetha.com (C.P.P.)

ABSTRACT

This study presents a sustainable and biocompatible approach for fabricating starch/PVA electrospun nanoscaffolds incorporated with ultrasonically synthesized copper oxide nanoparticles (CuO NPs) derived from *Sargassum wightii* extract. The green-synthesized CuO NPs exhibited a surface plasmon resonance peak at 292 nm (UV-Vis), while Fourier-transform infrared spectroscopy (FTIR) confirmed the presence of stabilizing phytochemicals and successful integration into the nanoscaffold matrix. X-ray diffraction (XRD) analysis revealed a monoclinic tenorite phase for CuO NPs, whereas Scanning electron microscopy (SEM) imaging demonstrated uniform nanoparticle distribution within the fibrous scaffold. Thermogravimetric analysis (TGA) indicated thermal stability up to 220°C, and Dynamic light scattering (DLS) confirmed colloidal stability with a zeta potential of −120 mV. *In vitro* anticancer activity against HT-29 colon and MCF-7 breast cancer cells demonstrated dose-dependent cytotoxicity, with starch/PVA/CuO-NPs nanoscaffolds exhibiting the highest potency (IC_{50}: ~12 µg/mL for HT-29; ~18 µg/mL for MCF-7), outperforming standalone CuO NPs and algal extract. The enhanced efficacy is attributed to synergistic interactions between the polymer matrix and nanoparticles, promoting reactive oxygen species generation. These findings underscore the potential of eco-friendly nanoscaffolds as promising anticancer agents, warranting further mechanistic and *in vivo* studies.

KEYWORDS: *Sargassum wightii*, Green synthesis, CuO NPs, Starch/PVA/CuO-NPs nanoscaffolds, Anticancer activity.

1. INTRODUCTION

In recent years, the pursuit of sustainable, biocompatible, and cost-effective strategies for fabricating nanostructured biomaterials has gained immense traction in the field of nanomedicine [1]. Among various nanotechnological platforms, electrospun nanofibrous scaffolds have emerged as promising candidates for biomedical applications due to their structural similarity to the extracellular matrix (ECM), high surface area-to-volume ratio, and tunable mechanical properties [2]. When reinforced with bioactive nanoparticles, these scaffolds can be transformed into potent therapeutic systems for drug delivery and tissue regeneration [3]. Copper oxide nanoparticles (CuO NPs), in particular, have attracted widespread attention owing to their notable antimicrobial, antioxidant, and anticancer activities [4]. However, conventional methods of CuO NPs synthesis often involve harsh chemicals and energy-intensive procedures, which raise significant concerns regarding environmental sustainability and cytocompatibility [5].

To address these issues, green synthesis methods have been increasingly adopted, offering eco-friendly, low-cost, and biocompatible alternatives [6]. Among the various biological entities employed for nanoparticle synthesis, marine algae have demonstrated exceptional potential due to their abundant secondary metabolites, such as polyphenols, flavonoids, terpenoids, and polysaccharides, which act as natural reducing and stabilizing agents [7]. *Sargassum wightii*, a brown marine macroalga commonly found along the southern coast of India, particularly in the Rameswaram region, is a rich source of such bioactive compounds [8]. Previous studies have documented its antioxidant, anti-inflammatory, and anticancer properties, making it a compelling candidate for green nanomaterial synthesis [9]. The ultrasonic-assisted extraction technique further enhances the yield and activity of

the phytochemicals by disrupting the cell walls, facilitating better diffusion of intracellular components into the extraction medium [10].

In the context of scaffold fabrication, biopolymers such as starch and polyvinyl alcohol (PVA) are gaining prominence due to their biocompatibility, biodegradability, and ease of processing [11]. Starch, derived from renewable sources, offers excellent film-forming and hydrophilic properties, while PVA provides mechanical strength, chemical stability, and processability suitable for electrospinning [12]. When combined, these polymers form a synergistic matrix that can efficiently incorporate bioactive nanoparticles without compromising their physicochemical integrity [13]. The integration of CuO NPs into starch/PVA nanofibers may provide a dual advantage—enhancing the mechanical and functional properties of the scaffold while enabling sustained and localized anticancer activity [14].

The choice of electrospinning as the fabrication technique is deliberate, as it facilitates the creation of nanofibers with controlled diameters, high porosity, and uniform distribution of embedded nanoparticles [15]. This technique also allows for fine-tuning of process parameters to obtain scaffolds with desired morphologies and drug-release characteristics [16]. Moreover, the nanofibrous structure mimics the fibrous ECM, providing an ideal environment for cellular adhesion, proliferation, and differentiation [17]. By embedding CuO NPs synthesized via green chemistry into these electrospun matrices, a multifunctional scaffold can be developed that not only supports tissue architecture but also actively combats cancer cells through cytotoxic effects [18].

Cancer remains one of the leading causes of mortality globally, with colorectal and breast cancers representing significant proportions of new cases each year [19]. The limitations of conventional chemotherapy—such as systemic toxicity, drug resistance, and lack of specificity—underscore the urgent need for novel therapeutic platforms that are both effective and biocompatible [20]. Nanoparticle-based systems have shown promise in overcoming these challenges by enabling targeted delivery and minimizing off-target effects [21]. In this context, CuO NPs have demonstrated selective cytotoxicity against cancer cells through the generation of reactive oxygen species (ROS), disruption of mitochondrial membrane potential, and induction of apoptosis pathways [22]. However, their colloidal stability, controlled delivery, and biocompatibility need to be improved for successful *in vitro* and *in vivo* applications [23]. The use of a starch/PVA electrospun scaffold as a delivery matrix may offer an effective solution by providing a stable, biocompatible environment for the CuO NPs and facilitating their gradual release at the tumor site [14].

This study is rooted in the convergence of green nanotechnology and biomaterials science, with the primary aim of developing an eco-friendly, bioactive scaffold for potential anticancer therapy [24]. Herein, CuO NPs were synthesized using an ultrasonic-assisted green method employing *S wightii* extract, thereby eliminating the need for hazardous chemicals [25]. The synthesized nanoparticles were subsequently incorporated into a starch/PVA matrix via electrospinning to fabricate nanofibrous scaffolds [26]. Comprehensive physicochemical characterization of the nanoparticles and scaffolds was carried out using UV–Vis spectroscopy, Fourier-transform infrared spectroscopy (FTIR), X-ray diffraction (XRD), Scanning electron microscopy (SEM), Thermogravimetric analysis (TGA), zeta potential, and dynamic light scattering (DLS) analyses [27]. The anticancer potential of the developed scaffolds was evaluated *in vitro* using MTT assay against two widely studied human cancer cell lines—HT-29 (colorectal adenocarcinoma) and MCF-7 (breast carcinoma) [28]. The findings provide insights into the cytotoxic mechanisms of CuO-based scaffolds and offer a promising strategy for their application in cancer treatment [29].

2. MATERIALS AND METHODS

2.1. Materials

In this study, *S wightii*, a marine brown macroalga collected from the coastal waters of Rameswaram, Tamil Nadu, India, was utilized as a biological reducing agent for synthesizing CuO NPs. Copper (II) sulfate pentahydrate ($CuSO_4 \cdot 5H_2O$), procured from Sigma-Aldrich, was used as the precursor salt. PVA with an approximate molecular weight of 115,000 served as the main polymer for electrospinning. Commercially available starch was integrated to improve the structural properties of the scaffold. All chemicals used, including Milli-Q water and ethanol, were of analytical grade and sourced from Merck and Sigma-Aldrich. Electrospinning was performed using the HOLMARC HO-NFES-040 unit coupled with a syringe pump. Analytical characterization of the nanoparticles and scaffolds was conducted using UV-Vis spectroscopy (VIS SPEC V-730), FTIR (PerkinElmer Spectrum Two), XRD (Bruker D8 Advance), SEM (JSM-IT800 NANO), DLS and zeta potential (Malvern Zetasizer Ultra), and TGA (PerkinElmer TGA 8000). HT-29 colon and MCF-7 breast cancer cells were obtained from the National Centre for Cell Science (NCCS), Pune, India, which provided authenticated and contamination-free cell stocks for biological investigations focused on anticancer activity.

2.2. Collection of marine macroalgae

Fresh *S. wightii* specimens were harvested from nearshore marine zones around Rameswaram. The collected *Sargassum Wightii* was taxonomically identified and authenticated by Dr V. Veeragurunathan, CSIR-CSMCRI-Marine Algal Research Station, Mandapam Camp 623519, Tamil Nadu, India. A voucher specimen was prepared and deposited at the Herbarium of the CSIR-CSMCRI-Marine Algal Research Station, under the accession number:

SI–2025–RMM–017. This authentication ensures botanical accuracy and standardization of the study material. The collected algae were thoroughly rinsed with tap water to remove extraneous matter such as sand, microalgae, and detritus, followed by repeated washing with distilled water to ensure cleanliness. Approximately 100 grams of the cleaned macroalgae were cut into smaller segments and left to air-dry at room temperature for about two weeks. The dried algal biomass was then pulverized into a fine powder using a mechanical grinder and kept in sealed containers under dry conditions until further experimental use.

2.3. Ultrasonic-assisted extraction

To obtain bioactive compounds from the algae, 2 grams of the powdered *S. wightii* were dispersed in 50 mL of Milli-Q water in a 100 mL glass beaker. The mixture underwent ultrasonic treatment using a LABQUEST ultrasonic cleaner (Borosil; Serial No. 941032329018) maintained at 60°C for 45 minutes. After sonication, the mixture was filtered through Whatman No. 1 filter paper under aseptic conditions, and the filtrate was collected and stored at 10°C. For long-term storage and later applications, the extract was freeze-dried using a lyophilization system to obtain it in powder form [30, 31].

2.4. Green synthesis of CuO NPs

CuO NPs were synthesized via a green route using the aqueous extract of *S. wightii*. Specifically, 50 mL of 0.1 M $CuSO_4 \cdot 5H_2O$ solution was combined with 10 mL of algal extract (from 10 mg powder dissolved in 10 mL of Milli-Q water) at a 5:1 volume ratio. The resulting solution was stirred continuously at 650 rpm and maintained at 60°C for 2 hours. A noticeable shift in color from blue to bluish-green signified the onset of nanoparticle formation. The resultant product was centrifuged and washed three times using distilled water to eliminate unreacted residues. The purified CuO NPs were then freeze-dried for 48 hours and stored in powder form for further analysis and scaffold integration [32].

2.5. Fabrication of CuO-loaded electrospun Starch/PVA scaffolds

A 15% (w/w) aqueous solution of PVA was prepared by dissolving the polymer in Milli-Q water under constant agitation. Following this, 100 mg each of starch and CuO NPs were added to the solution, and the mixture was stirred thoroughly at 50°C for 2.5 hours to ensure uniform dispersion. The homogenous solution was then loaded into a syringe fitted with a 0.84 mm inner diameter needle and processed using a HOLMARC HO-NFES-040 electrospinning unit connected to a HMPSKV30 high-voltage power supply (0–30 kV, 0.5 mA). Optimized parameters included an applied voltage of 11.5 kV, a tip-to-collector distance of 12.3 cm, and a solution feed rate of 0.4 mL/h. Electrospinning was continued for 6 to 8 hours at ambient conditions to fabricate nanofibrous mats [33-35].

2.6. Physicochemical characterization

2.6.1. UV–visible spectroscopy

UV-Vis spectrophotometry was used to validate the synthesis of CuO NPs and assess the optical properties of the algal extract and synthesized NPs. Absorbance readings were recorded in the 200–800 nm range using the VIS SPEC V-730, with deionized water as the blank. Characteristic absorption peaks indicated the surface plasmon resonance and confirmed the incorporation of nanoparticles in the electrospun scaffold [36].

2.6.2. FTIR spectroscopy analysis

FTIR spectra were captured using a PerkinElmer Spectrum Two operating in ATR mode to identify functional groups and molecular interactions. Each sample was scanned over the 4000–400 cm^{-1} range at a 4 cm^{-1} resolution with 64 accumulations. Peaks corresponding to hydroxyl, carbonyl, amide, and metal-oxygen groups were interpreted to understand the interactions between scaffold components and nanoparticles [37].

2.6.3. XRD analysis

Crystalline structure analysis of CuO NPs and nanofibrous scaffolds was conducted using a Bruker D8 Advance diffractometer with CuKα radiation ($\lambda = 1.5406$ Å), operated at 40 kV and 40 mA. Data were recorded over a 2θ range of 5°–90°, using a 0.029649° step size. Diffraction peaks corresponding to monoclinic CuO were identified, and changes in peak patterns were noted to detect interactions with the polymeric matrix [38].

2.6.4. SEM analysis

The surface topography, fiber morphology, and particle dispersion within the scaffolds were examined using JEOL JSM-IT800 NANO SEM. Samples were sputter-coated with gold before imaging to prevent electron charging. High-resolution images provided detailed insights into the fibrous architecture and nanoparticle incorporation [39].

2.6.5. TGA analysis

Thermal behavior and decomposition stages of the samples were assessed using the PerkinElmer TGA 8000. Approximately 5 mg of each sample was subjected to a temperature ramp from room temperature to 550°C at 15°C/min under a nitrogen atmosphere. The resulting thermograms indicated moisture evaporation, material degradation, and overall thermal stability [40].

2.6.6. Zeta potential and DLS

DLS and zeta potential analyses were performed using the Malvern Zetasizer Ultra to determine the particle size distribution and surface charge of the synthesized CuO NPs. These data offered insights into the stability and colloidal behavior of the nanoparticle suspensions in aqueous environments [41].

All primary data and processed results have been deposited in the Mendeley Data repository (DOI: 10.17632/vf8822rd8j.2) for transparency and reproducibility.

2.7. *In Vitro* anticancer activity

2.7.1. Cell lines and culture conditions

The HT-29 (Human Colorectal Adenocarcinoma) and MCF-7 (Human Breast Cancer) cell lines were acquired from the National Center for Cell Science (NCCS), Pune, India. The cells were cultured as per standard NCCS protocols using Minimum Essential Medium (MEM) supplemented with 10% fetal bovine serum (FBS). The cultures were maintained in a humidified incubator at 37°C with 5% CO_2 atmosphere [28].

2.7.2. MTT assay for cell viability

HT-29 and MCF-7 cells were seeded at a density of 5×10^5 cells per well in 96-well microplates and incubated overnight for adherence. The cells were then treated with serial concentrations (6.25, 12.5, 25, 50, and 100 µg/mL) of algal extract, CuO NPs, and starch/PVA/CuO-NPs scaffolds in triplicates. After 24 hours of incubation at 37°C in 5% CO_2, MTT solution was added and incubated for another 4 hours. The formazan crystals formed were dissolved in 200 µL DMSO, and absorbance was read at 570 nm using a microplate reader. Experiments were independently repeated three times to ensure data reliability. The average OD values and standard deviations were computed for each treatment group to determine cytotoxic efficacy [42].

2.8. Statistical analysis

Data from all experiments were statistically evaluated using SPSS version 25.0 and GraphPad Prism version 9.0. Results are presented as mean ± standard deviation from triplicate measurements. Statistical differences between groups were assessed using one-way ANOVA followed by suitable post hoc tests such as Tukey's or Dunnett's. A p-value less than 0.05 was considered statistically significant. Pearson's correlation was applied to identify associations among variables. The Shapiro–Wilk test was used to examine data normality, and any datasets that did not meet normal distribution assumptions were log-transformed. All statistical interpretations were carried out with a 95% confidence level to ensure robustness [43].

3. RESULTS

3.1. UV–visible spectroscopy

The UV–Visible spectral analysis (Fig. 1) of the aqueous extract from *S wightii* and the synthesized CuO NPs confirmed the successful formation of nanoparticles and provided insights into their optical characteristics. The algal extract exhibited a prominent absorption peak at 346 nm, which can be attributed to the presence of phytochemicals such as flavonoids and polyphenols. These compounds likely play dual roles as reducing and stabilizing agents during the nanoparticle synthesis process. In contrast, the CuO NPs demonstrated a distinct absorption peak at 292 nm, indicative of surface plasmon resonance (SPR), a hallmark of nanoparticle formation. Additionally, a broad absorption band spanning 400–800 nm was observed, potentially signifying particle aggregation or interactions within the matrix. Measurements were conducted using a VIS SPEC V-730 spectrophotometer over a wavelength range of 200–800 nm, with deionized water serving as the reference. The absence of extraneous peaks suggests a high purity of the synthesized nanoparticles. The observed SPR behavior aligns with known optical properties of metal oxide nanoparticles, underscoring the efficacy of *S. wightii* extract in facilitating nanoparticle synthesis.

3.2. FTIR spectroscopy analysis

FTIR spectroscopy (Fig. 2) was employed to elucidate the functional groups present in both the CuO NPs and the starch/PVA electrospun nanoscaffolds. Spectra were recorded using a PerkinElmer Spectrum Two spectrometer operating in attenuated total reflectance (ATR) mode, covering the range of 4000–400 cm^{-1} with a resolution of 4 cm^{-1} over 64 scans. The CuO NP spectrum revealed eleven significant bands corresponding to various functional groups involved in nanoparticle stabilization and metal-oxygen bonding. In the nanoscaffold spectrum, prominent peaks were observed at 3298.42 cm^{-1} (O–H/N–H stretching vibrations), 2924.17 cm^{-1} (C–H stretching in aliphatic chains), 1710.48 cm^{-1} (C=O stretching), 1426.82 cm^{-1} (C–H bending or COO^- symmetric stretching), and 1097.57 cm^{-1} (C–O–C or Si–O–Si vibrations). Additional minor peaks at 1329.64, 919.55, and 843.63 cm^{-1} were associated with C–N stretching, P–O–C linkages, or Cu–O vibrations, confirming the successful incorporation of CuO NPs into the scaffold. Shifts in peak positions and the broadening of bands, coupled with the absence of impurity signals, suggest strong interactions between the nanoparticles and the polymer matrix, likely mediated through hydrogen bonding or electrostatic forces. These spectral features indicate a diverse array of functional groups within the scaffold and effective nanoparticle integration, which may influence its mechanical, biological, and catalytic properties.

3.3. XRD analysis

XRD patterns (Fig. 3) of the CuO NPs and the starch/PVA nanoscaffold were obtained using a Bruker D8 Advance diffractometer equipped with CuKα radiation (λ = 1.5406 Å), operating at 40 kV and 40 mA. Data were collected over a 2θ range of 5° to 90°, with a step size of 0.029649°. The CuO NPs exhibited 32 sharp diffraction peaks, notably at 16.386° (5.405 Å), 22.406° (3.965 Å), 24.107° (3.689 Å), 31.894° (2.804 Å), 32.745° (2.733 Å), 38.307° (2.348 Å), and 48.057° (1.892 Å), corresponding to the monoclinic tenorite phase of CuO (JCPDS 05-0661). The

intense peaks at 22.406° and 24.107°, with relative intensities of 80.2% and 100% respectively, confirm the crystalline nature of the nanoparticles. The broadening of these peaks suggests nanoscale crystallite sizes. The diffraction pattern of the nanoscaffold indicated a semi-crystalline structure, comprising 45.3% crystalline and 54.7% amorphous regions. Peaks at 29.372° (3.038 Å), 38.502° (2.336 Å), and 44.687° (2.026 Å) were attributed to embedded CuO, with minor shifts (e.g., 38.502° vs. 38.307°) and reduced intensity indicating interactions with the polymer matrix. Full width at half maximum (FWHM) values ranged from 0.130° to 0.341° for the scaffold and 0.115° to 0.580° for the CuO NPs, reflecting variations in crystal size and strain. The absence of foreign peaks confirms the high purity of the samples, while the broadening of scaffold peaks suggests reduced crystallinity due to polymer incorporation. Overall, these findings validate the successful synthesis of CuO NPs and their effective integration into a structurally coherent scaffold with tailored crystallinity suitable for biomedical or catalytic applications.

3.4. SEM analysis

SEM imaging (Fig. 4) was performed using a JEOL JSM-IT800 NANO microscope to examine the morphology of the CuO NPs and the starch/PVA nanoscaffolds. Prior to imaging, samples were sputter-coated with gold to minimize surface charging. The CuO NPs appeared as uniformly spherical particles, indicating precise synthesis with minimal aggregation. The electrospun scaffolds displayed a porous, fibrous network, confirming optimal electrospinning conditions. CuO NPs were evenly distributed across the fiber surfaces without noticeable aggregation, which is crucial for consistent scaffold performance. The nanofibers exhibited smooth, bead-free regions, reflecting stable polymer jet behavior during electrospinning. These morphological features suggest a scaffold architecture conducive to cell adhesion and nutrient exchange, while the uniform dispersion of CuO NPs supports enhanced antimicrobial or catalytic activity. Collectively, the SEM observations highlight the scaffold's potential in tissue engineering and drug delivery applications, where nanostructural uniformity and stability are essential.

3.5. TGA analysis

TGA (Fig. 5) of the starch/PVA electrospun scaffolds was conducted using a PerkinElmer TGA 8000 under a nitrogen atmosphere. A 5.518 mg sample was heated from room temperature to 550°C at a rate of 15°C per minute. The thermal profile revealed a multi-phase degradation process. An initial mass loss occurred below 150°C, attributed to the evaporation of moisture. The primary degradation phase spanned from an onset temperature of 220.95°C to an end temperature of 382.16°C, with a peak degradation rate at 322.94°C. This phase corresponds to the breakdown of starch and PVA polymer chains, including the degradation of hydroxyl and glycosidic structures, resulting in a 37.126% weight reduction. Beyond 382.16°C, no significant weight change was observed, indicating the thermal stability of residuals and embedded CuO NPs. These results demonstrate that the scaffold maintains thermal stability up to approximately 220°C, making it suitable for sterilization and handling processes. The degradation behavior aligns with that of conventional starch/PVA systems, with the presence of CuO potentially enhancing thermal stability, although further studies are needed to elucidate its influence on the final residue characteristics.

3.6. Zeta potential and particle size

DLS and zeta potential analyses of the CuO NPs were performed using a Malvern Zetasizer Ultra to assess dispersion stability and particle size in aqueous media. DLS measurements indicated a monodisperse distribution with a mean hydrodynamic diameter of 146.1 nm (Fig. 6), confirming uniform nanoparticle sizing. The zeta potential measurement revealed a strong negative value of −120 mV (Fig. 7), suggesting significant electrostatic repulsion between particles, which inhibits aggregation and enhances colloidal stability. Typically, a zeta potential magnitude exceeding ±30 mV is indicative of long-term dispersion stability, a critical factor for applications in catalysis and biomedicine. The narrow size distribution and pronounced negative surface charge reflect efficient synthesis and surface modification, likely resulting from biomolecular capping during the green synthesis process. Overall, these findings confirm that the CuO NPs possess favorable physicochemical properties for stable aqueous dispersion and functional performance.

3.7. *In Vitro* anticancer activity

The algal extract, CuO NPs, and starch/PVA/CuO-NPs nanoscaffolds exhibited dose-dependent cytotoxicity against the HT-29 colon cancer cell line. At the lowest concentration (6.25 µg/mL), the algal extract demonstrated high cell viability (95.9%), while CuO NPs and nanoscaffolds showed reduced viability (80.9% and 77.3%, respectively). As the concentration increased to 100 µg/mL, the algal extract reduced viability to 34.7%, whereas CuO NPs and nanoscaffolds further decreased viability to 24.2% and 17.3%, respectively. The IC_{50} values (concentration required to inhibit 50% of cell growth) were determined as follows: Algal extract: ~35 µg/mL, CuO NPs: ~15 µg/mL and Starch/PVA/CuO-NPs nanoscaffolds: ~12 µg/mL. These results indicate that the nanoscaffolds possessed the highest cytotoxic potency against HT-29 cells, followed by CuO NPs, while the algal extract exhibited moderate activity.

A similar trend was observed in the MCF-7 breast cancer cell line. At 6.25 µg/mL, the algal extract maintained 97.7% cell viability, whereas CuO NPs and nanoscaffolds reduced viability to 87.2% and 80.8%, respectively. At the highest concentration (100 µg/mL), the algal extract decreased viability to 48.5%, while CuO NPs and

nanoscaffolds further suppressed viability to 39.9% and 26.8%, respectively. The IC_{50} values were calculated as: Algal extract: ~50 µg/mL, CuO NPs: ~20 µg/mL and Starch/PVA/CuO-NPs nanoscaffolds: ~18 µg/mL. The nanoscaffolds again demonstrated superior anticancer activity compared to CuO NPs and the algal extract, suggesting enhanced efficacy in targeting breast cancer cells.

Both cell lines exhibited greater sensitivity to the nanoscaffolds, likely due to the synergistic effects of the starch/PVA matrix and CuO NPs, which enhance cellular uptake and reactive oxygen species (ROS) generation. The algal extract showed moderate activity, possibly due to the presence of bioactive compounds with slower cytotoxic mechanisms. CuO NPs displayed intermediate potency, aligning with their known ability to induce oxidative stress in cancer cells. These findings highlight the potential of starch/PVA/CuO-NPs nanoscaffolds as a promising anticancer agent, warranting further investigation into their mechanistic pathways and *in vivo* efficacy.

4. DISCUSSION

The UV–Visible spectroscopy analysis presented compelling evidence for the successful biosynthesis of CuO NPs utilizing the aqueous extract of *S wightii*. The algal extract's absorption peak at 346 nm corresponds to the characteristic presence of polyphenols and flavonoids, well-known phytochemicals that act as natural reducing and stabilizing agents during green nanoparticle synthesis. This aligns with previous findings in green synthesis literature where plant and algal extracts facilitate nanoparticle formation through these bioactive compounds. The distinct surface plasmon resonance (SPR) peak observed at 292 nm for CuO NPs is a clear indicator of nanoparticle formation, consistent with the optical behavior of metal oxide nanoparticles. Moreover, the broad absorption band detected between 400 and 800 nm might suggest nanoparticle aggregation or intermolecular interactions within the colloidal system, a phenomenon that can be influenced by particle size, shape, and surface chemistry. The absence of additional peaks confirms the high purity of the nanoparticles, reinforcing the efficiency of *S wightii* extract as both a reducing and capping agent [44-46].

FTIR spectroscopy further substantiated the involvement of various functional groups in nanoparticle synthesis and stabilization. The characteristic vibrational bands in the CuO NP spectrum, alongside the starch/PVA electrospun scaffold, reveal strong chemical interactions between the nanoparticles and the polymer matrix. Notably, the broad peak around 3298 cm^{-1} indicates hydrogen bonding and possibly electrostatic interactions between hydroxyl and amine groups of the polymers and the nanoparticle surface. The shifts and broadening of bands such as C=O, C–H, and Cu–O vibrations confirm that CuO NPs were successfully embedded within the starch/PVA matrix. These interactions are crucial, as they can enhance the mechanical integrity, thermal stability, and biological performance of the nanoscaffolds. The interplay of these functional groups likely contributes to the scaffold's multifunctional properties, such as improved antimicrobial activity and biocompatibility [47, 48].

XRD analysis validated the crystalline nature of the synthesized CuO NPs, exhibiting peaks matching the monoclinic tenorite phase of copper oxide, which is consistent with established JCPDS standards. The peak broadening observed in the XRD patterns suggests nanoscale particle dimensions, typical for materials synthesized via green methods, where particle size control is often influenced by extract concentration and reaction conditions. Importantly, the starch/PVA nanoscaffold displayed a semi-crystalline profile with a notable proportion of amorphous content, a common characteristic for polymer-based composites. The presence of CuO-specific peaks within the scaffold's diffraction pattern with slight shifts in peak position and reduced intensity indicates successful integration of the nanoparticles into the polymer matrix without altering their crystalline structure substantially. This semi-crystalline nature is advantageous for biomedical applications, as it offers a balance between mechanical strength and flexibility, critical for scaffold performance in tissue engineering and drug delivery [41, 49].

Morphological characterization through SEM provided visual confirmation of the uniformity and quality of both the CuO NPs and the electrospun nanofibers. The spherical morphology of CuO NPs with minimal aggregation suggests controlled nucleation and growth during biosynthesis. Within the scaffold, the well-distributed nanoparticles across the smooth, bead-free nanofibers highlight optimal electrospinning parameters and effective nanoparticle dispersion. This morphology not only supports mechanical robustness but also enhances the surface area available for biological interactions, which is vital for cellular adhesion and nutrient exchange in tissue scaffolds. The porous architecture observed is particularly important for facilitating oxygen diffusion and waste removal, which may contribute to enhanced cell viability and proliferation in future *in vitro* or *in vivo* studies. Moreover, the absence of nanoparticle aggregation within the scaffold matrix suggests strong nanoparticle-polymer interactions, aligning with the FTIR results [50, 51].

The thermal stability profile obtained from TGA analysis revealed that the starch/PVA nanoscaffolds maintain integrity up to approximately 220°C, which is suitable for many biomedical processing conditions, including sterilization. The multi-phase degradation pattern corresponds well with the thermal breakdown of polymer chains, confirming the expected behavior of starch and PVA composites. The residual mass plateau beyond 382°C is likely attributable to the inorganic CuO content, which imparts enhanced thermal stability to the scaffold. This improved stability is beneficial for maintaining scaffold structure under physiological and processing stresses, thus extending the potential application range of these materials. However, further detailed studies are required to

quantify the exact role of CuO in modifying thermal degradation kinetics and to explore potential synergies in composite behavior [52-54].

DLS and zeta potential measurements demonstrated that the CuO nanoparticles possess a uniform size distribution with an average hydrodynamic diameter around 146 nm, confirming nanoscale dimensions suitable for biomedical applications. The strongly negative zeta potential (−120 mV) indicates excellent colloidal stability due to significant electrostatic repulsion, which is crucial for preventing nanoparticle aggregation in aqueous environments. Such stability enhances their dispersion within polymer matrices and biological media, improving bioavailability and cellular uptake. The negative surface charge likely results from biomolecular capping agents present in the *S* extract, which not only stabilize nanoparticles but might also contribute to their biological activity by mediating interactions with cellular membranes [55, 56].

The anticancer activity assays revealed that starch/PVA/CuO nanoscaffolds exerted the most potent cytotoxic effects against HT-29 colon and MCF-7 breast cancer cells compared to the extract and CuO NPs alone. The dose-dependent decrease in cell viability and lower IC_{50} values for nanoscaffolds suggest a synergistic effect between the polymer matrix and embedded CuO NPs. This enhanced cytotoxicity might be attributed to improved cellular internalization of nanoparticles facilitated by the scaffold architecture and the generation of reactive oxygen species (ROS) by CuO, leading to oxidative stress-induced apoptosis in cancer cells. The polymer matrix possibly aids in controlled release and localized concentration of CuO, increasing therapeutic efficacy while potentially minimizing systemic toxicity. In contrast, the algal extract alone exhibited moderate activity, likely due to slower or less potent bioactive compound delivery. These promising *in vitro* results highlight the potential of the nanoscaffolds as a platform for targeted cancer therapy and warrant further mechanistic studies and *in vivo* evaluations to fully elucidate their anticancer mechanisms and biocompatibility [57, 58].

5. CONCLUSION

This study successfully demonstrated the green synthesis of CuO NPs using *S wightii* aqueous extract, confirming their formation and stability through comprehensive spectroscopic, microscopic, and thermal analyses. The integration of CuO NPs into starch/PVA electrospun nanoscaffolds was achieved effectively, as evidenced by FTIR, XRD, and SEM data, revealing strong interactions between the nanoparticles and polymer matrix and resulting in a structurally coherent and thermally stable composite. The nanoscaffolds exhibited uniform morphology with well-dispersed CuO NPs, promoting favorable properties for biomedical applications. Importantly, the starch/PVA/CuO-NPs nanoscaffolds showed enhanced *in vitro* anticancer activity against HT-29 and MCF-7 cell lines compared to the algal extract and CuO NPs alone, suggesting a synergistic effect improving cytotoxic efficacy. These findings highlight the potential of these green-synthesized nanocomposites as promising candidates for cancer therapy, encouraging further mechanistic studies and *in vivo* evaluations to validate their clinical applicability.

Ethics declaration: Not Applicable

Data Availability Statement: The full dataset of physiochemical characterization associated with this work is published in Mendeley Data **[Dataset]** Eco-conscious biomaterial design: Analytical insights into starch nanoscaffolds with green-engineered copper oxide nanoparticles using marine *Sargassum wightii* extract (DOI: 10.17632/vf8822rd8j.1). Disclosure: The material characterization data and figures (e.g., UV, SEM, FTIR, XRD, TGA, Zeta Potential and particle sizer) presented here were generated from a common dataset and are being reused across multiple related studies on nanomaterials. All biological analyses and conclusions are original to each manuscript.

Conflicts of Interest: The authors declare no conflicts of interest.

REFERENCES

1. Harun-Ur-Rashid M, Jahan I, Foyez T, Imran AB. Bio-inspired nanomaterials for micro/nanodevices: a new era in biomedical applications. Micromachines. 2023;14(9):1786.
2. Chaka KT, Cao K, Tesfaye T, Qin X. Nanomaterial-functionalized electrospun scaffolds for tissue engineering. Journal of Biomaterials Science, Polymer Edition. 2025;36(3):371-413.
3. Sharma S, Sudhakara P, Singh J, Ilyas R, Asyraf M, Razman M. Critical review of biodegradable and bioactive polymer composites for bone tissue engineering and drug delivery applications. Polymers. 2021;13(16):2623.
4. Maliki M, Ifijen IH, Ikhuoria EU, Jonathan EM, Onaiwu GE, Archibong UD, et al. Copper nanoparticles and their oxides: optical, anticancer and antibacterial properties. International Nano Letters. 2022;12(4):379-98.
5. Pourmadadi M, Holghoomi R, Maleki-baladi R, Rahdar A, Pandey S. Copper nanoparticles from chemical, physical, and green synthesis to medicinal application: a review. Plant Nano Biology. 2024:100070.
6. Gupta D, Boora A, Thakur A, Gupta TK. Green and sustainable synthesis of nanomaterials: recent advancements and limitations. Environmental Research. 2023;231:116316.

7. AlNadhari S, Al-Enazi NM, Alshehrei F, Ameen F. A review on biogenic synthesis of metal nanoparticles using marine algae and its applications. Environmental Research. 2021;194:110672.
8. Afreen A, Rasool F, Fatima M. Bioactive properties of brown seaweed, Sargassum wightii and its nutritional, therapeutic potential and health benefits: A review. Journal of Environmental Biology. 2023;44(2):146-58.
9. Elsaffany AH, Abdelaziz AE, Zahra AA, Mekky AE. Green synthesis of silver nanoparticles using cocoon extract of Bombyx mori L.: therapeutic potential in antibacterial, antioxidant, anti-inflammatory, and anti-tumor applications. BMC biotechnology. 2025;25(1):1-17.
10. Liu Y, Liu X, Cui Y, Yuan W. Ultrasound for microalgal cell disruption and product extraction: A review. Ultrasonics Sonochemistry. 2022;87:106054.
11. Saini T, Meena J, Verma V, Saini S, Malik R. Polyvinyl Alcohol: Recent Advances and Applications in Sustainable Materials. Polymer-Plastics Technology and Materials. 2025:1-32.
12. Pan W, Liang Q, Gao Q. Preparation of hydroxypropyl starch/polyvinyl alcohol composite nanofibers films and improvement of hydrophobic properties. International Journal of Biological Macromolecules. 2022;223:1297-307.
13. Elmowafy M, Shalaby K, Elkomy MH, Alsaidan OA, Gomaa HA, Abdelgawad MA, et al. Polymeric nanoparticles for delivery of natural bioactive agents: recent advances and challenges. Polymers. 2023;15(5):1123.
14. Uzair B, Syed N, Kanwal A, Samin G, Niazi MBK, Abbas S, et al. Synthesis of AgO/CuO/PVA/starch hydrogel by casting method and characterizations to safely overcome skin infections: A possible application in wound healing as a dressing. Materials Today Communications. 2024;39:109286.
15. Liu R, Hou L, Yue G, Li H, Zhang J, Liu J, et al. Progress of fabrication and applications of electrospun hierarchically porous nanofibers. Advanced Fiber Materials. 2022;4(4):604-30.
16. Capuana E, Lopresti F, Carfì Pavia F, Brucato V, La Carrubba V. Solution-based processing for scaffold fabrication in tissue engineering applications: A brief review. Polymers. 2021;13(13):2041.
17. Ahmadian E, Eftekhari A, Janas D, Vahedi P. Nanofiber scaffolds based on extracellular matrix for articular cartilage engineering: a perspective. Nanotheranostics. 2023;7(1):61.
18. Radulescu D-M, Andronescu E, Vasile OR, Ficai A, Vasile BS. Silk fibroin-based scaffolds for wound healing applications with metal oxide nanoparticles. J Drug Deliv Sci Technol. 2024:105689.
19. Morgan E, Arnold M, Gini A, Lorenzoni V, Cabasag C, Laversanne M, et al. Global burden of colorectal cancer in 2020 and 2040: incidence and mortality estimates from GLOBOCAN. Gut. 2023;72(2):338-44.
20. Eslami M, Memarsadeghi O, Davarpanah A, Arti A, Nayernia K, Behnam B. Overcoming chemotherapy resistance in metastatic cancer: a comprehensive review. Biomedicines. 2024;12(1):183.
21. Hristova-Panusheva K, Xenodochidis C, Georgieva M, Krasteva N. Nanoparticle-mediated drug delivery systems for precision targeting in oncology. Pharmaceuticals. 2024;17(6):677.
22. Ahamed M, Lateef R, Akhtar MJ, Rajanahalli P. Dietary antioxidant curcumin mitigates CuO nanoparticle-induced cytotoxicity through the oxidative stress pathway in human placental cells. Molecules. 2022;27(21):7378.
23. Singh N, Qutub S, Khashab NM. Biocompatibility and biodegradability of metal organic frameworks for biomedical applications. Journal of Materials Chemistry B. 2021;9(30):5925-34.
24. Mahmud MZA, Islam MD, Mobarak MH. The Development of Eco-Friendly Biopolymers for Use in Tissue Engineering and Drug Delivery. Journal of Nanomaterials. 2023;2023(1):9270064.
25. Guirguis HA, Farghal HH, Yang H, Shoeib T, El-Sayed MM. Algal-mediated nanotechnology for environmental and biochemical applications. Biogenic Nanomaterial for Health and Environment. 2023:140-59.
26. García G, Moreno-Serna V, Saavedra M, Cordoba A, Canales D, Alfaro A, et al. Electrospun scaffolds based on a PCL/starch blend reinforced with CaO nanoparticles for bone tissue engineering. International Journal of Biological Macromolecules. 2024;273:132891.
27. Elgharbawy H, Hassona A, Morsy R. Synthesis and biophysical characterization of porous bi-phase calcium phosphate/gelatin-PVA scaffold: enhanced antibacterial, osteoconductivity and anticancer activity via silver nanoparticles and methotrexate incorporation. Journal of Molecular Structure. 2024;1311:138329.
28. Hazhir N, Chekin F, Raoof JB, Fathi S. Anticancer activity of Doxorubicin conjugated to polymer/carbon based-nanohybrid against MCF-7 breast and HT-29 colon cancer cells. International Journal of Nano Dimension. 2021;12(1).
29. preet Singh G, Singh J, Chandel K, Arora S, Singh S, Singh D, et al. Synthesis and characterization of pristine CuO and Mg/CuO nanostructures for their anti-breast cancer and photocatalytic degradation applications: Experimental and DFT investigations. Materials Today Communications. 2024;40:109398.
30. Martins R, Mouro C, Pontes R, Nunes J, Gouveia I. Ultrasound-assisted extraction of bioactive pigments from Spirulina platensis in natural deep eutectic solvents. Bioresources and Bioprocessing. 2023;10(1):88.
31. Martín-del-Campo A, Fermín-Jiménez JA, Fernández-Escamilla VV, Escalante-García ZY, Macías-Rodríguez ME, Estrada-Girón Y. Improved extraction of carrageenan from red seaweed (Chondracantus canaliculatus) using ultrasound-assisted methods and evaluation of the yield, physicochemical properties and functional groups. Food Science and Biotechnology. 2021;30:901-10.

32. Anbalagan G, Subramanian B, Suresh V, Sivaperumal P. Green synthesis of copper and copper oxide nanoparticles from brown algae turbinaria species' aqueous extract and its antibacterial properties. Cureus. 2024;16(4).
33. Filimon A, Dobos AM, Onofrei MD, Serbezeanu D. Polyvinyl Alcohol-Based Membranes: A Review of Research Progress on Design and Predictive Modeling of Properties for Targeted Application. Polymers. 2025;17(8):1016.
34. Sunarwidhi AL, Hernawan A, Frediansyah A, Widyastuti S, Martyasari NWR, Abidin AS, et al. Multivariate analysis revealed ultrasonic-assisted extraction improves anti-melanoma activity of non-flavonoid compounds in indonesian brown algae ethanol extract. Molecules. 2022;27(21):7509.
35. Rahman Khan MM, Rumon MMH, Islam M. Synthesis, Rheology, Morphology, and Mechanical Properties of Biodegradable PVA-Based Composite Films: A Review on Recent Progress. Processes. 2024;12(12).
36. Rajkumar M, Presley SD, Govindaraj P, Kirubakaran D, Farahim F, Ali T, et al. Synthesis of chitosan/PVA/copper oxide nanocomposite using Anacardium occidentale extract and evaluating its antioxidant, antibacterial, anti-inflammatory and cytotoxic activities. Sci Rep. 2025;15(1):3931.
37. Truzzi E, Marchetti L, Bertelli D, Benvenuti S. Attenuated total reflectance–Fourier transform infrared (ATR–FTIR) spectroscopy coupled with chemometric analysis for detection and quantification of adulteration in lavender and citronella essential oils. Phytochemical analysis. 2021;32(6):907-20.
38. Jaison JP, Balasubramanian B, Gangwar J, Pappuswamy M, Meyyazhagan A, Kamyab H, et al. Bioactive nanoparticles derived from marine brown seaweeds and their biological applications: a review. Bioprocess and Biosystems Engineering. 2024;47(10):1605-18.
39. Ullah H, Usman F, Rasheed MA, Khan AA, Ahmad R, Lee SY, et al. Anodic SnO2 nanoporous channels functionalized with CuO quantum dots for selective H2O2 biosensing. ACS Applied Nano Materials. 2022;5(7):9096-111.
40. Safari P, Rahimabadi EZ, Vaezi MR, Behnamghader A, Tahergorabi R. Development of ZnO-NPs reinforced chitosan nanofiber mats with improved antibacterial and biocompatibility properties. Sci Rep. 2025;15(1):1-17.
41. Mobarak MB, Hossain MS, Chowdhury F, Ahmed S. Synthesis and characterization of CuO nanoparticles utilizing waste fish scale and exploitation of XRD peak profile analysis for approximating the structural parameters. Arabian Journal of Chemistry. 2022;15(10):104117.
42. Duarte D, Cardoso A, Vale N. Synergistic growth inhibition of HT-29 colon and MCF-7 breast cancer cells with simultaneous and sequential combinations of antineoplastics and CNS drugs. International Journal of Molecular Sciences. 2021;22(14):7408.
43. Gulcin İ, Alwasel SH. DPPH radical scavenging assay. Processes. 2023;11(8):2248.
44. Hasan EA, El-Hashash MA, Zahran MK, El-Rafie HM. Comparative study of chemical composition, antioxidant and anticancer activities of both Turbinaria decurrens Bory methanol extract and its biosynthesized gold nanoparticles. Journal of Drug Delivery Science and Technology. 2022;67:103005.
45. Wamsley M, Zou S, Zhang D. Advancing evidence-based data interpretation in UV–Vis and fluorescence analysis for nanomaterials: an analytical chemistry perspective. Analytical chemistry. 2023;95(48):17426-37.
46. Roshanbinfar K, Evans AD, Samanta S, Kolesnik-Gray M, Fiedler M, Krstic V, et al. Enhancing biofabrication: Shrink-resistant collagen-hyaluronan composite hydrogel for tissue engineering and 3D bioprinting applications. Biomaterials. 2025;318:123174.
47. Nandiyanto ABD, Ragadhita R, Fiandini M. Interpretation of Fourier transform infrared spectra (FTIR): A practical approach in the polymer/plastic thermal decomposition. Indonesian Journal of Science and Technology. 2023;8(1):113-26.
48. Pasieczna-Patkowska S, Cichy M, Flieger J. Application of Fourier Transform Infrared (FTIR) Spectroscopy in Characterization of Green Synthesized Nanoparticles. Molecules. 2025;30(3):684.
49. Badry R, El-Nahass MM, Nada N, Elhaes H, Ibrahim MA. Structural and UV-blocking properties of carboxymethyl cellulose sodium/CuO nanocomposite films. Sci Rep. 2023;13(1):1123.
50. Zhang Y, Zhang M, Cheng D, Xu S, Du C, Xie L, et al. Applications of electrospun scaffolds with enlarged pores in tissue engineering. Biomaterials Science. 2022;10(6):1423-47.
51. Nandee R, Chowdhury MA, Hossain N, Rana MM, Mobarak MH, Khandaker MR. Surface topography and surface morphology of graphene nanocomposite by FESEM, EDX and AFM analysis. Nano-Structures & Nano-Objects. 2024;38:101170.
52. Chandel S, Pandey P, Saini S, Sharma R, Parashar B, Yadav K. Natural Product-Loaded PCL and PLA-Based Bio-Scaffold and Their Applications. Natural Product Inspired Scaffolds: Applications in Tissue Engineering. Springer; 2024. p. 117-46.
53. Le TDH, Tuan HNA, Nguyen VT, Le AT. Hydroxyapatite− loaded starch/polyvinyl alcohol scaffold for bone regeneration application: preparation and characterization. Journal of Sol-Gel Science and Technology. 2023;107(2):441-51.
54. Ramezani M, Ripin ZM. An overview of enhancing the performance of medical implants with nanocomposites. Journal of Composites Science. 2023;7(5):199.

55. Alizadeh SR, Ebrahimzadeh MA. Characterization and anticancer activities of green synthesized CuO nanoparticles, a review. Anti-Cancer Agents in Medicinal Chemistry (Formerly Current Medicinal Chemistry-Anti-Cancer Agents). 2021;21(12):1529-43.
56. Weiss M, Fan J, Claudel M, Sonntag T, Didier P, Ronzani C, et al. Density of surface charge is a more predictive factor of the toxicity of cationic carbon nanoparticles than zeta potential. Journal of nanobiotechnology. 2021;19:1-19.
57. Bharathi DS, Boopathyraja A, Nachimuthu S, Kannan K. Green Synthesis, Characterization and antibacterial activity of SiO 2–ZnO nanocomposite by Dictyota bartayresiana extract and its cytotoxic effect on HT29 Cell Line. Journal of Cluster Science. 2022:1-17.
58. El-Moslamy SH, El-Maradny YA, El-Sayed MH, El-Sakhawy MA, El-Fakharany EM. Facile phyto-mediated synthesis of ternary CuO/Mn3O4/ZnO nanocomposite using Nigella Sativa seeds extract: characterization, antimicrobial, and biomedical evaluations. Sci Rep. 2025;15(1):1-21.

Figures

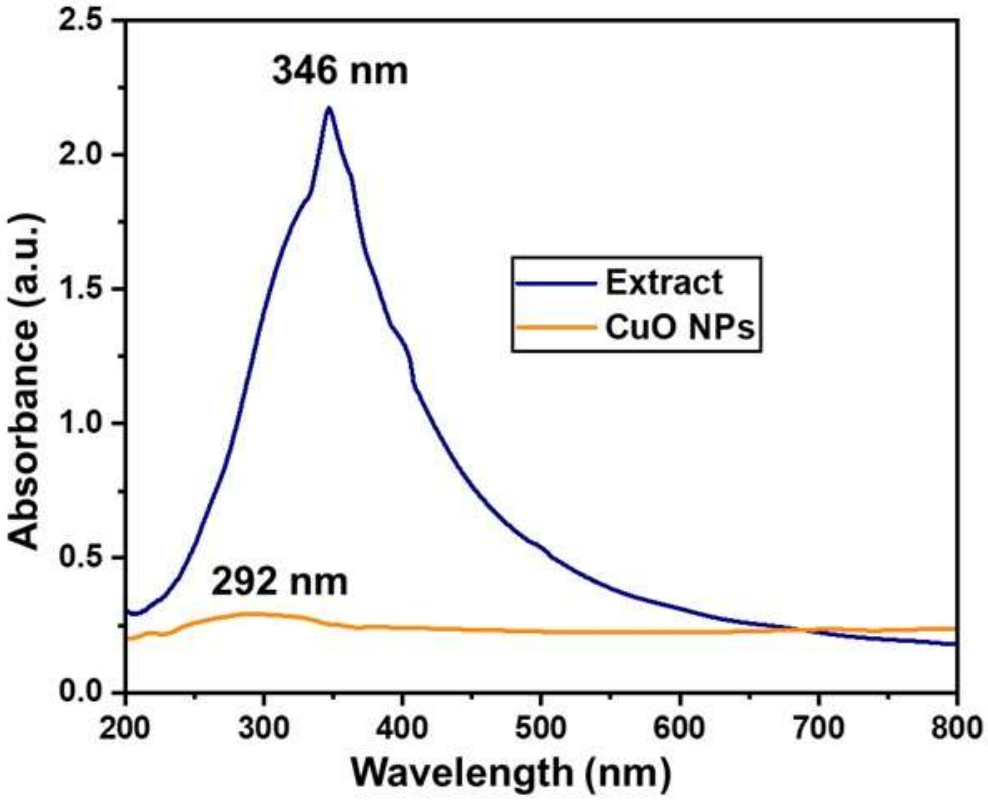

Fig. 1. UV–Visible spectral profiles of algal extract and CuO NPs.

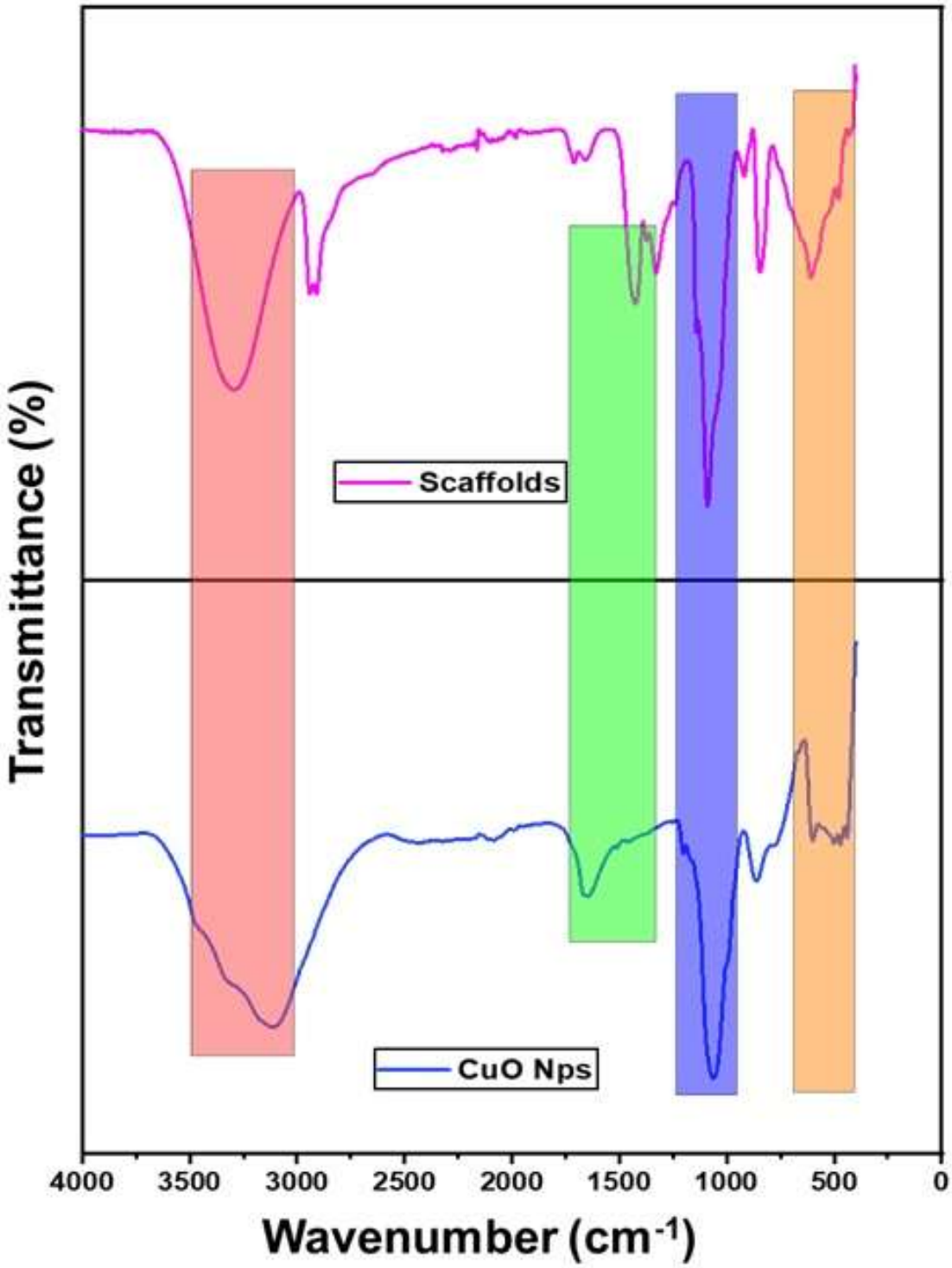

Fig. 2. FTIR spectra of CuO NPs and their incorporation into nanoscaffolds.

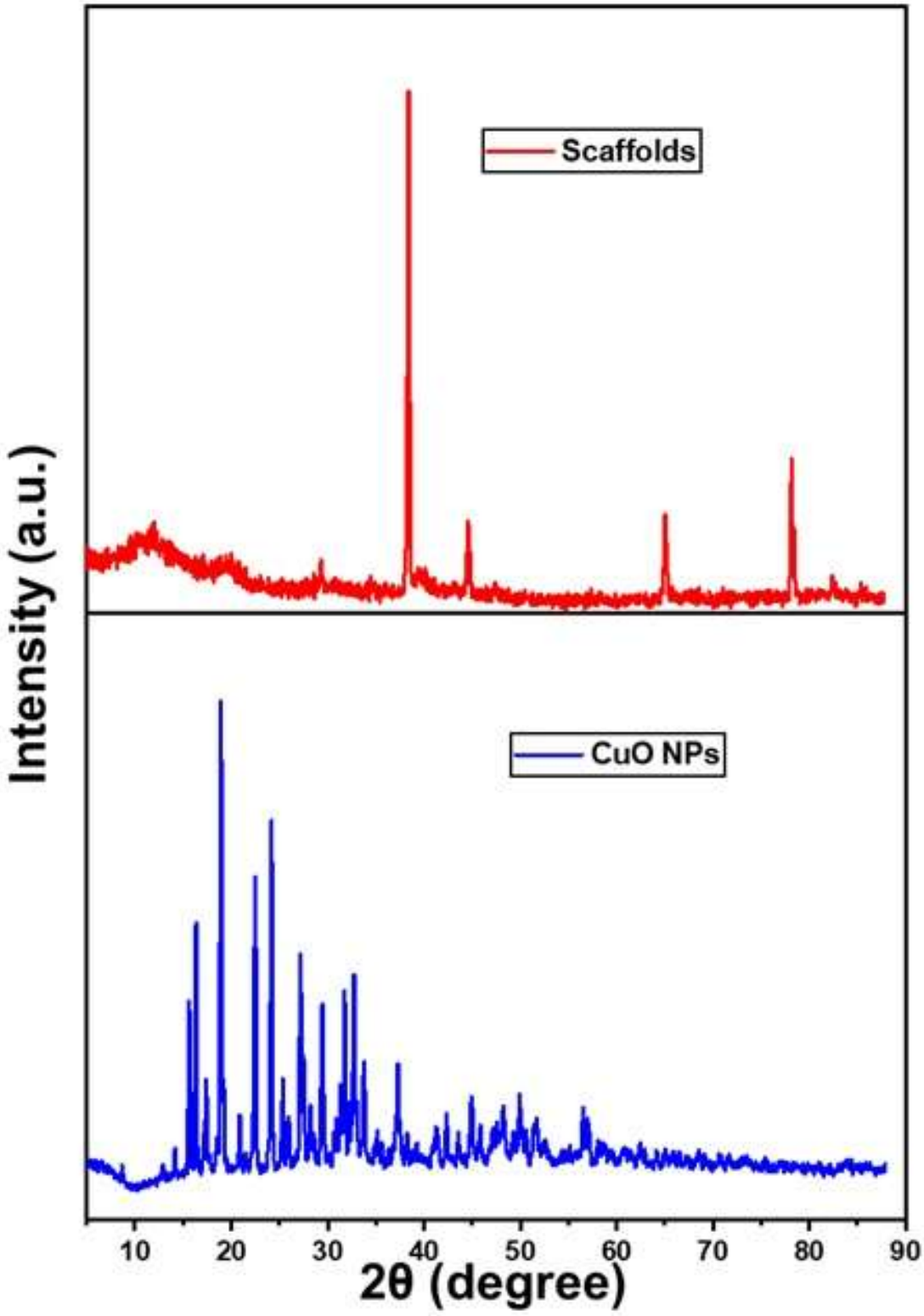

Fig. 3. XRD patterns of synthesized CuO NPs and CuO-loaded scaffolds.

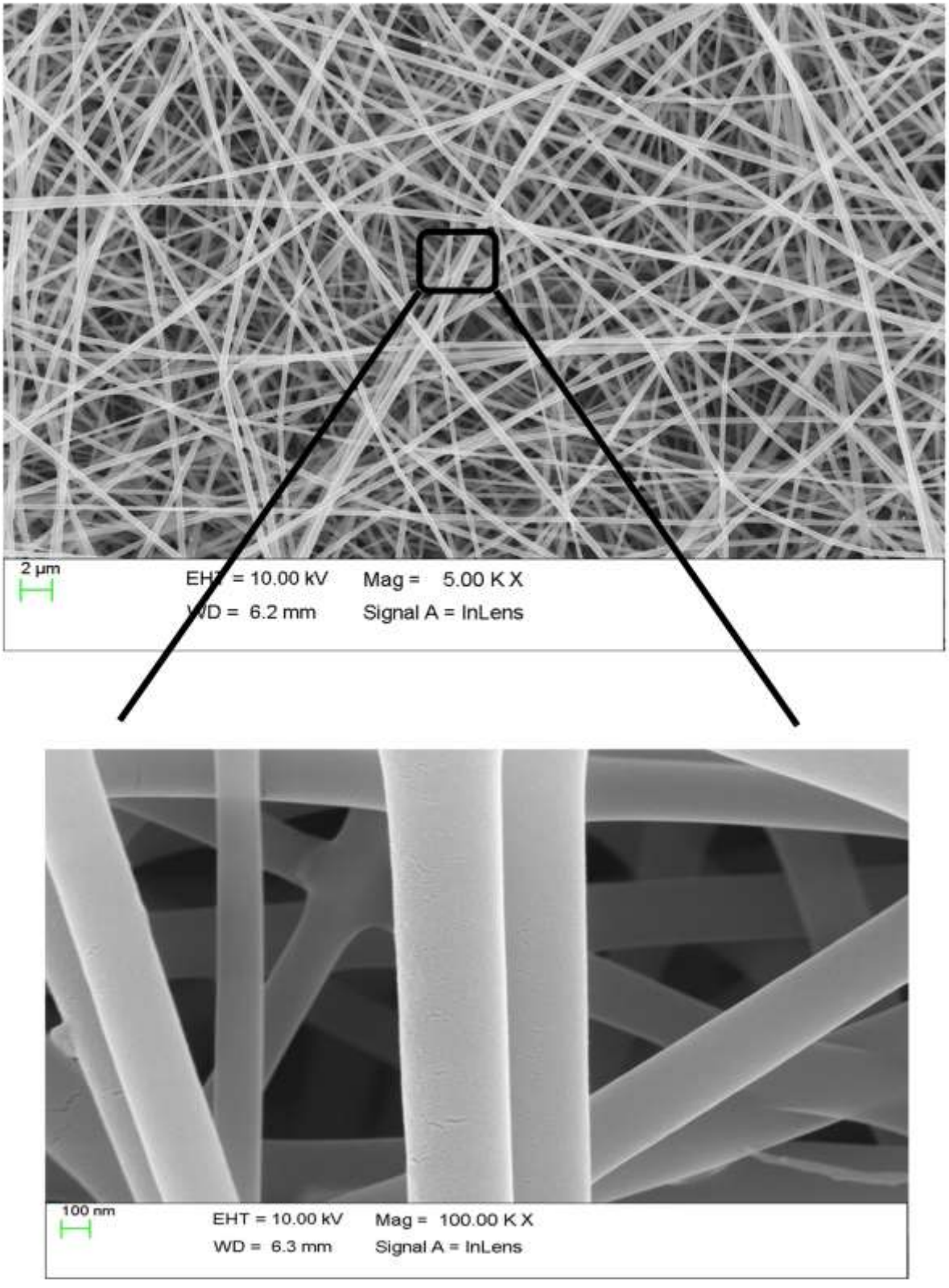

Fig. 4. SEM analysis of synthesized CuO NPs and CuO-loaded scaffolds.

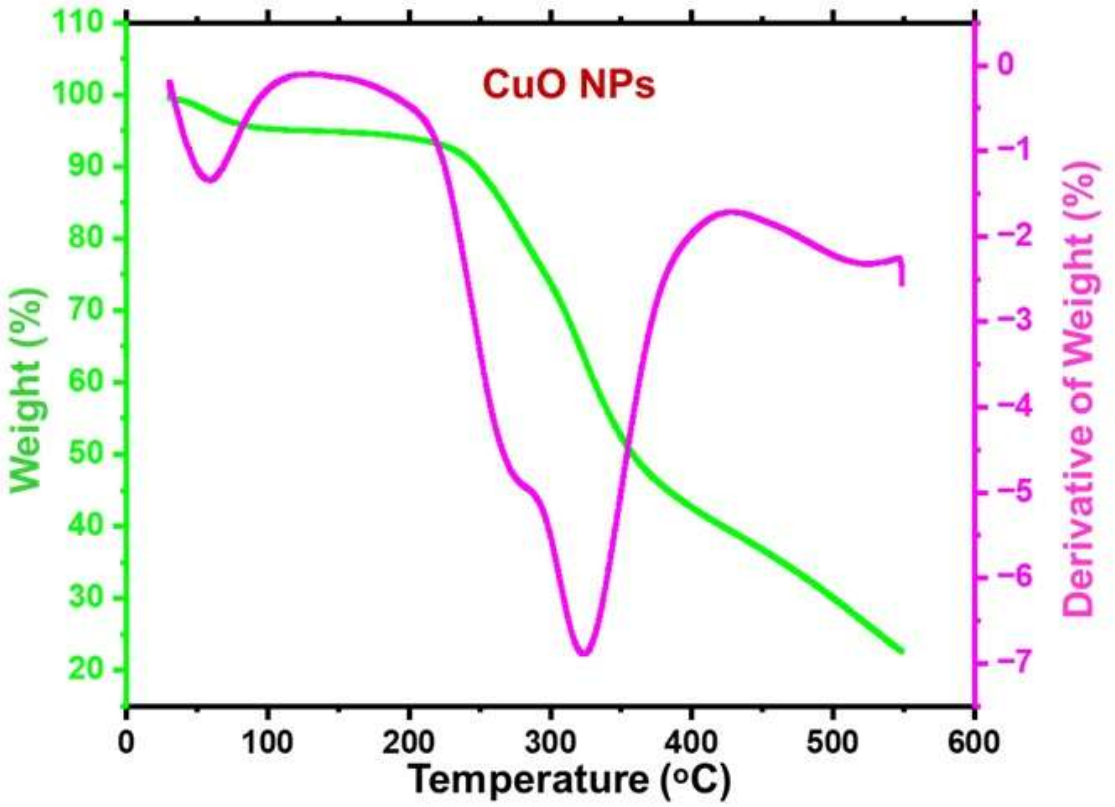

Fig. 5. Thermal degradation behavior of CuO-incorporated nanoscaffolds.

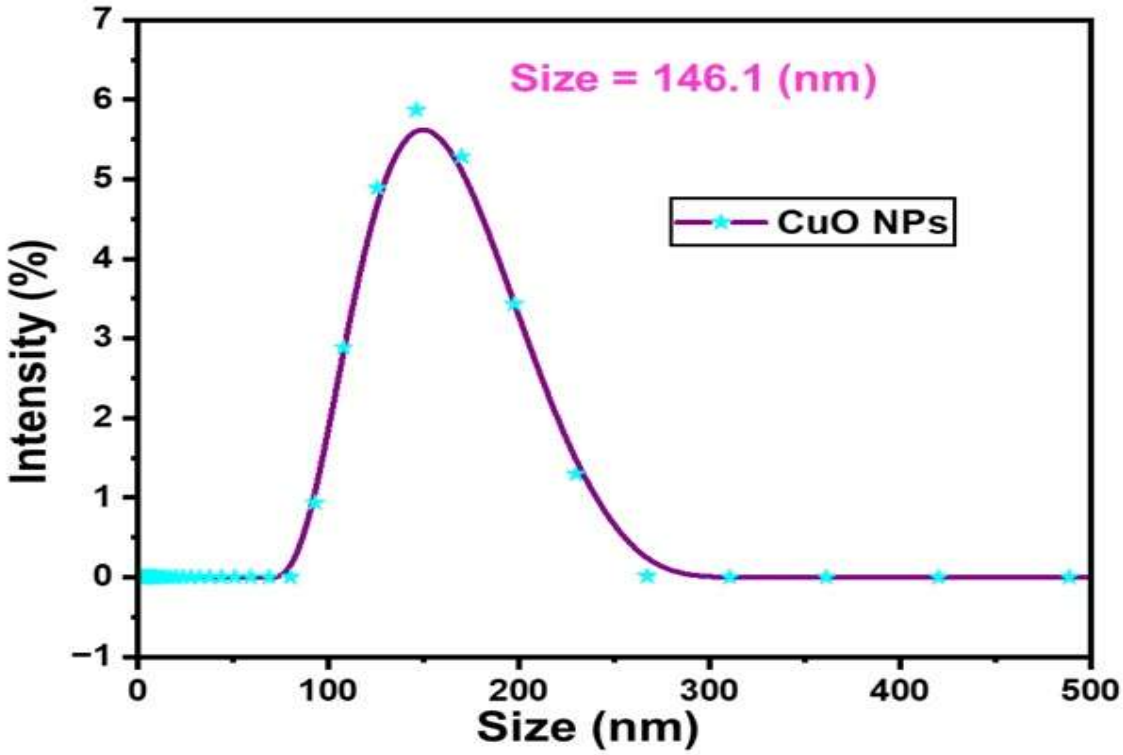

Fig. 6. DLS particles size analysis of CuO NPs

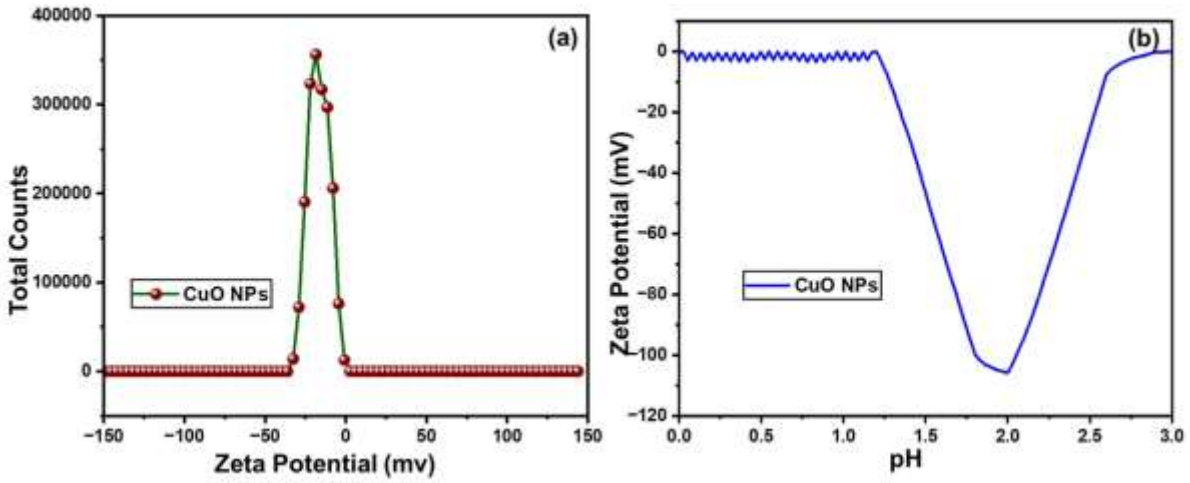

Fig. 7. Zeta-potential analysis of CuO NPs

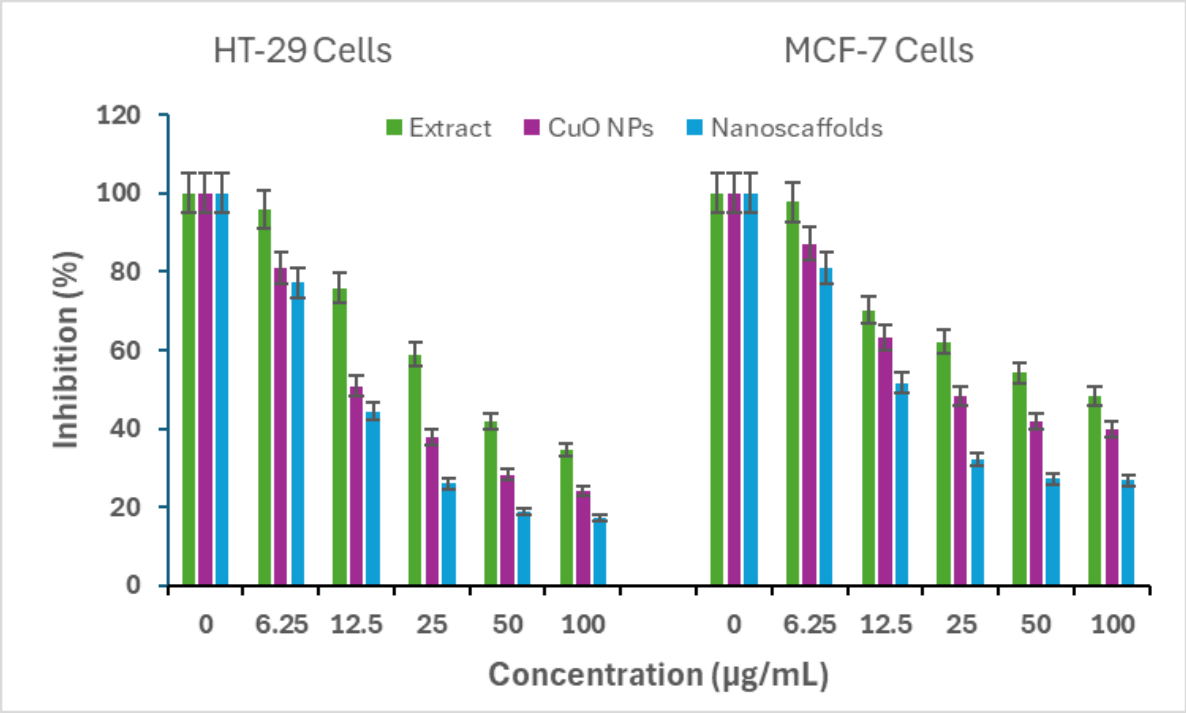

Fig. 8. Anticancer activity analysis of algal extract, CuO-NPs and starch/PVA/CuO-NPs nanoscaffolds